

# Geophysical Research Letters®



## RESEARCH LETTER

10.1029/2021GL095286

### Key Points:

- The 110 km long, 0.4–1.2 km maximum displacement, Bilila-Mtakataka Fault (BMF) locally follows shallow crustal weaknesses
- The BMF has limited fault gouge and a narrow damage zone compared to a similar displacement fault in intact crust
- Limited fracturing implies less seismic energy is consumed by fracture and frictional energy when ruptures follow pre-existing weaknesses

### Supporting Information:

Supporting Information may be found in the online version of this article.

### Correspondence to:

J. N. Williams,  
jack.williams@otago.ac.nz

### Citation:

Williams, J. N., Fagereng, Å., Wedmore, L. N. J., Biggs, J., Mdala, H., Mphepo, F., & Hodge, M. (2022). Low dissipation of earthquake energy where a fault follows pre-existing weaknesses: Field and microstructural observations of Malawi's Bilila-Mtakataka Fault. *Geophysical Research Letters*, 49, e2021GL095286. <https://doi.org/10.1029/2021GL095286>

Received 20 JUL 2021  
Accepted 28 MAR 2022

### Author Contributions:

**Conceptualization:** Jack N. Williams, Åke Fagereng, Juliet Biggs, Michael Hodge  
**Formal analysis:** Jack N. Williams, Felix Mphepo  
**Funding acquisition:** Åke Fagereng, Juliet Biggs  
**Investigation:** Jack N. Williams, Åke Fagereng, Luke N. J. Wedmore, Hassan Mdala, Felix Mphepo, Michael Hodge  
**Methodology:** Jack N. Williams, Åke Fagereng, Luke N. J. Wedmore

© 2022. The Authors.

This is an open access article under the terms of the [Creative Commons Attribution License](https://creativecommons.org/licenses/by/4.0/), which permits use, distribution and reproduction in any medium, provided the original work is properly cited.

## Low Dissipation of Earthquake Energy Where a Fault Follows Pre-Existing Weaknesses: Field and Microstructural Observations of Malawi's Bilila-Mtakataka Fault

Jack N. Williams<sup>1,2,3</sup> , Åke Fagereng<sup>1</sup> , Luke N. J. Wedmore<sup>3</sup> , Juliet Biggs<sup>3</sup> , Hassan Mdala<sup>4</sup>, Felix Mphepo<sup>4</sup>, and Michael Hodge<sup>1</sup> 

<sup>1</sup>School of Earth and Environmental Sciences, Cardiff University, Cardiff, UK, <sup>2</sup>Now at the Department of Geology, University of Otago, Dunedin, New Zealand, <sup>3</sup>School of Earth Sciences, University of Bristol, Bristol, UK, <sup>4</sup>Geological Survey Department, Mzuzu Regional Office, Mzuzu, Malawi

**Abstract** During earthquakes on low (<1–2 km) displacement faults in isotropic crust, more earthquake energy is consumed by fracturing and gouge formation than in ruptures along more mature faults. To investigate how pre-existing weaknesses affect earthquake energy dissipation along low displacement faults, we studied fault rocks from the 110 km long, 0.4–1.2 km displacement, Bilila-Mtakataka Fault (BMF), Malawi. Where the BMF is parallel to surface metamorphic fabrics, macroscale fractures define a narrow (5–20 m wide) damage zone relative to where the BMF is foliation-oblique (20–80 m), and to faults with comparable displacement in isotropic crust (~40–120 m). Enhanced microfracturing and widespread gouge formation, typically reported from comparable-displacement faults, are not observed. Therefore, minimal evidence for earthquake energy dissipation into the BMF's surrounding wall rock exists, despite geomorphic evidence for  $M_w$  7.5–8 earthquakes. We attribute this finding to differences in earthquake energy partitioning along incipient faults in isotropic and anisotropic crust.

**Plain Language Summary** Earthquakes release elastic energy stored in the Earth's crust. Some of this energy radiates to the Earth's surface, where it causes the ground to shake and poses a risk to human life and infrastructure. However, some of this energy is also absorbed by breaking and fragmenting the rocks around the fault. This process is important in faults with small total displacements (<1–2 km), because these faults are still growing by breaking surrounding intact rock. The Bilila-Mtakataka Fault (BMF) in southern Malawi is 110 km long but has a low displacement (0.4–1.2 km). We show that limited fracturing of the surrounding rock has occurred, despite an inferred history of  $M_w$  7.5–8 earthquakes. We propose that this is because earthquakes along the BMF exploited older planes of weakness in the Earth's crust, such as cracks and aligned mineral grains. Our results suggests that these pre-existing weaknesses can influence how earthquake energy is released.

## 1. Introduction

Pre-existing mechanical weaknesses in the crust, such as joints, bedding planes, and metamorphic fabrics can profoundly affect earthquake rupture propagation (Allen, 2005; Hecker et al., 2021; Heermance et al., 2003; Yang et al., 2021). Over multiple earthquake cycles, these weaknesses can therefore influence the progressive development of fault rocks and wall rock fracturing, and hence fault strength and permeability (Butler et al., 2008; Crider & Peacock, 2004). Furthermore, in continental rifts, normal faults that reactivate pre-existing weaknesses can lengthen rapidly (Collanega et al., 2019; Hecker et al., 2021; Paton, 2006; Walsh et al., 2002). Therefore, interactions between pre-existing crustal weaknesses and fault structure can affect seismic hazard (Heermance et al., 2003) and the extent to which fault zone fluid flow can focus minerals into economically viable deposits (Micklethwaite & Cox, 2004).

Fault zone structure is typically described by: (a) one or more relatively narrow "fault cores" that comprise fault breccias, cataclasites, and/or gouges, and can include one or more principal slip zones (Sibson, 1977), and (b) a surrounding "damage zone," where fracture density is high relative to the host rocks but shear displacements are small and the original protolith is preserved (Caine et al., 1996). Gouge formation and damage zone fracturing can occur in response to multiple processes such as quasi-static fault tip propagation (Lockner et al., 1991; Renard et al., 2018), chemical alteration (Lacroix et al., 2015), and when the energy released during an earthquake is partially absorbed by the surrounding crust, as described by:

**Project Administration:** Jack N. Williams, Åke Fagereng, Luke N. J. Wedmore, Juliet Biggs  
**Visualization:** Jack N. Williams, Juliet Biggs, Michael Hodge  
**Writing – original draft:** Jack N. Williams  
**Writing – review & editing:** Jack N. Williams, Åke Fagereng, Luke N. J. Wedmore, Juliet Biggs, Hassan Mdala, Felix Mphemo, Michael Hodge

$$E_T = (E_G + E_F) + E_R \quad (1)$$

where  $E_T$  is the total earthquake energy release,  $E_R$  is radiated seismic energy, and  $E_G$  and  $E_F$  are the energy required to create a slip surface (fracture energy) and slide along that surface (frictional energy) respectively (Kanamori & Rivera, 2006).  $E_G$  and  $E_F$  cannot be distinguished based on geological observations of fault zones; however, together these terms can be considered to represent dissipative processes that reduce the  $E_R$  available to reach the surface (Kanamori & Rivera, 2006; Shipton et al., 2006).

Several lines of evidence suggest that in isotropic crust, fault damage and gouge formation primarily occur during early fault growth. First, a scaling between damage zone width and total fault displacement is only observed for displacements <1–2 km (Savage & Brodsky, 2011; Torabi et al., 2020). Seismic waveforms, field observations, and gouge particle analysis also suggest that  $E_G$  and  $E_F$  account for a disproportionately high amount of  $E_T$  in earthquakes along low displacement faults (Chester et al., 2005; Kaneko et al., 2017; Ma et al., 2006; Niemeijer et al., 2012; Wilson et al., 2005). Finally, damage zone fracturing is particularly prevalent along geometrically complex faults (Bistacchi et al., 2010; Childs et al., 2009; Fang & Dunham, 2013; Perrin et al., 2016; Savage & Cooke, 2010; Tinti et al., 2005), and these complexities tend to be smoothed as faults accumulate displacement (Sagy et al., 2007).

The structural evolution of faults in anisotropic crust is, however, unclear, with examples of foliation-parallel faults that are narrower (Heermance et al., 2003; Wedmore et al., 2020; Zangerl et al., 2006) or of comparable or greater width (Bistacchi et al., 2010; Fletcher et al., 2020; Soden et al., 2014; Wheeler & Karson, 1989) than faults with equivalent displacement that cross-cuts foliation or are hosted in isotropic crust (Table S1 in the Supporting Information S1). These contrasting observations may reflect variations in confining pressures and temperatures (McBeck et al., 2019; Soden et al., 2014; Williams et al., 2018), relative orientations of the fault, mechanical weakness, and regional principal stresses (Donath, 1961; Fletcher et al., 2020; Misra et al., 2015; Tien et al., 2006), interseismic fault zone healing (Callahan et al., 2020; McBeck et al., 2021), the composition and spacing of fabrics (Beacom et al., 2001; Williams et al., 2018), and/or the presence of strain-hardening phyllosilicates (Bistacchi et al., 2010; Faulkner et al., 2008; Fletcher et al., 2020) and mechanically isotropic cataclastite (Kirkpatrick et al., 2013). Therefore, when investigating the structural evolution of faults in anisotropic crust, it is important that the influence of these factors can be separated.

Here, we investigate the Bilila-Mtakataka Fault (BMF), a 110 km long normal fault in southern Malawi with geomorphic evidence for Late Quaternary  $M_w$  7.5–8 earthquakes (Hodge et al., 2018, 2020; Jackson & Blenkinsop, 1997). The BMF provides important constraints on near-surface fault zone development in anisotropic crust as it shows variable geometrical relationships with surrounding Proterozoic metamorphic fabrics, and with a maximum displacement of 0.4–1.2 km, it represents a rare field example of an active crustal-scale low-displacement normal fault. Our field and microstructural analyses of the BMF can therefore document the effects of pre-existing anisotropies on earthquake energy dissipation around an incipient but >100 km long fault.

## 2. The Bilila-Mtakataka Fault

The BMF is situated in southern Malawi in the amagmatic Makanjira Graben, which geodetic models indicate accommodates ~0.7 mm/yr extension between the San and Rovuma plates near the southern end of the East African Rift's Western Branch (Figure 1; Wedmore et al., 2021). The BMF is expressed at the surface by an escarpment that juxtaposes Proterozoic Southern Irumide Belt gneisses in the footwall against hanging wall post-Miocene sediments. At the base of the escarpment is a continuous 128 km long (trace length), 5–28 m high soil-mantled scarp. Using topographic profiles, this scarp inferred to have formed in at least two  $M_w$  7.8 ± 0.3 earthquakes, with the most recent event likely occurring within the past 10,000 years (Hodge et al., 2018, 2020).

At scales of 0.1–10 km, variations in the scarp's height, strike, and/or orientation with respect to NW-SE striking amphibolite-granulite facies Southern Irumide Belt metamorphic fabrics have been used to divide the BMF into six 10–40 km long hard-linked sections (Figure 1; Hodge et al., 2018). It is unclear, however, if the BMF has grown from recent linkage of these sections (Cartwright et al., 1995), or if these sections were superimposed from interactions between near-surface foliations and up-dip fault propagation above a deeper-seated (depths >5 km) sub-planar weakness (Hodge et al., 2018).

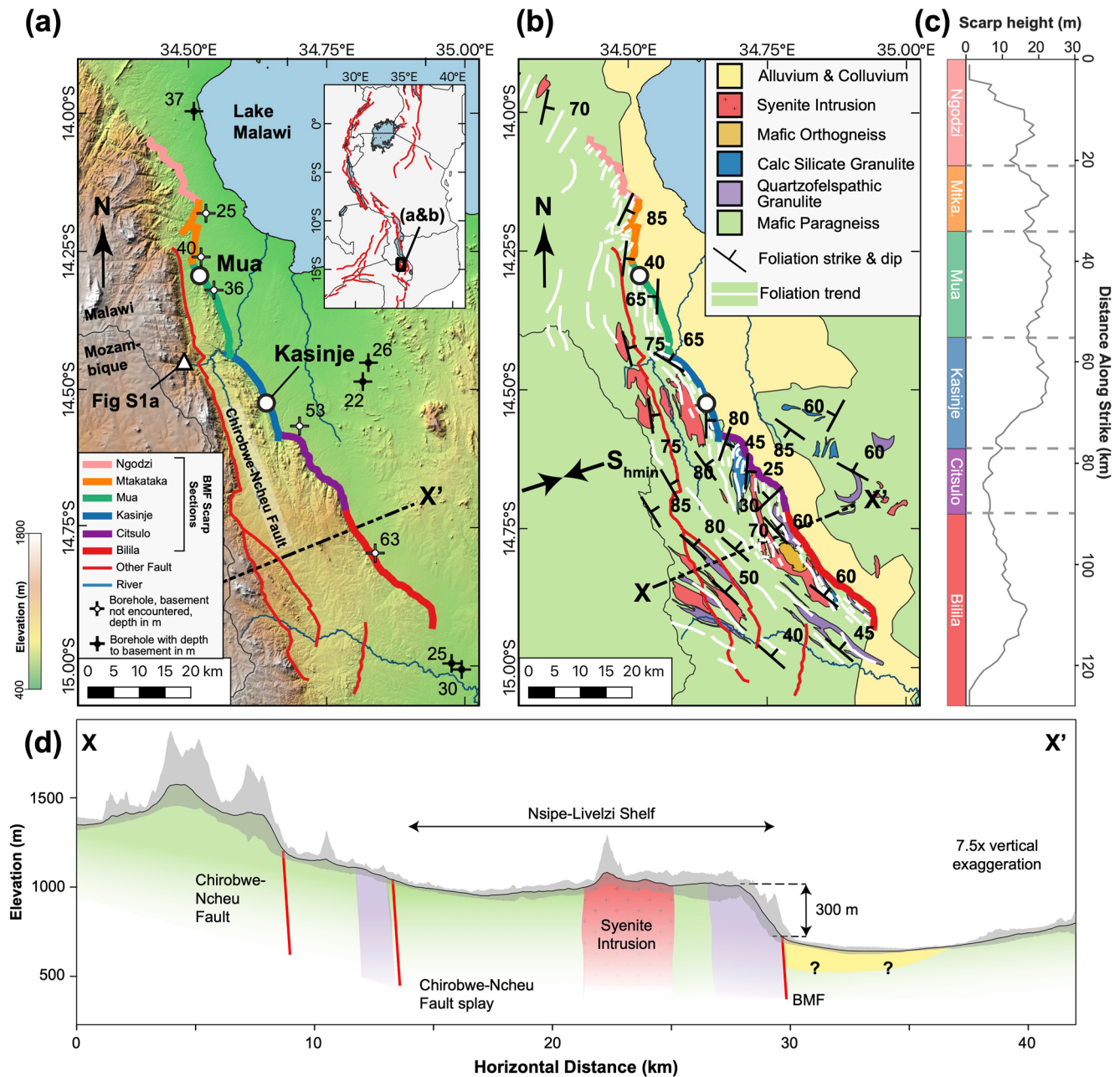


**Figure 1.** Geologic and geomorphic context of the Bilila-Mtakataka Fault (BMF). (a) The BMF scarp’s six sections (Hodge et al., 2018) underlain by a 12 m resolution TanDEM-X digital elevation model, and (b) its surrounding geologic units and foliation orientations (Dawson & Kirkpatrick, 1968; Hodge et al., 2018; Walshaw, 1965). Inset in (a), the BMF location in the context of the East African Rift.  $S_{hmin}$  in (b): azimuth of minimum horizontal stress from a focal mechanism stress inversion (Williams et al., 2019). (c) Along-strike scarp-height profile for the BMF measured from TanDEM-X data, and previously presented in Hodge et al. (2018). (d) Regional scale cross section through the BMF at the point of its maximum footwall relief, with key as in (b). Black line and shading represent mean and range of topography in a swath 2.5 km either side of the line shown in (b) (Schwanghart & Scherler, 2014).

The BMF’s total displacement, and its along-strike variability, is poorly constrained. This reflects limited constraints on hanging-wall sediment thickness and challenges with distinguishing between fault-related footwall exhumation and pre-existing topography imposed by lithologic variations (Figure 1). Nevertheless, an estimate of maximum displacement,  $D_{max}$ , can be made by considering the escarpment’s maximum height (~300 m, Figure 1), and that boreholes (Figure 1a; Dawson & Kirkpatrick, 1968; Walshaw, 1965), aeromagnetic data (Ojo et al., 2022), and the syn-rift sediment thickness across strike in Lake Malawi (Scholz et al., 2020) constrain

the maximum thickness of hanging-wall sediments to be 50–500 m. Assuming that the BMF hanging-wall and footwall cut-offs are represented by the base of the synrift sediments and the top of the escarpment (Accardo et al., 2018), the maximum throw across the BMF is therefore 350–800 m. When projected through its estimated dip (42–60°; Hodge et al., 2018; Stevens et al., 2021), we therefore constrain its  $D_{\max}$  to be 0.4–1.2 km, and given a fault length ( $L$ ) of 110 km, the  $D_{\max}:L$  ratio is 0.004–0.011. This low  $D_{\max}:L$  ratio indicates that the BMF is in its early growth stages, regardless of whether it grew through segment linkage (Cartwright et al., 1995; Rotevatn et al., 2019) or by attaining its full length near instantaneously (Walsh et al., 2002).

### 3. Field and Microstructural Observations

Samples and structural measurements were collected along two rivers oriented approximately perpendicular to the BMF scarp near the villages of Kasinje and Mua (Figures 1–3, Table S2 in the Supporting Information S1). These sites were chosen because they represent locations with fault-parallel and fault-oblique foliations. Microstructural investigations were made with a petrological microscope on thin sections cut perpendicular to a foliation where present. To quantify fracture density in these samples, we measured the length of intra- and inter-granular microfractures in quartz and feldspar grains in three 8–15 mm<sup>2</sup> areas per sample using FracPaQ v2.2 (Healy et al., 2017), and then divided the total microfracture length by the region's quartzofeldspathic grain area (Wedmore et al., 2020). Grain boundary fractures were not included in this analysis. Backscatter electron imaging and Energy Dispersive Spectroscopy (EDS) analyses were also performed on selected samples (Table S2 in the Supporting Information S1) using a Zeiss Sigma HD Field Emission Gun Analytical Scanning Electron Microscope (SEM) in the School of Earth and Environmental Sciences at Cardiff University. Samples were coated with 10 nm of carbon, and the SEM data were acquired with a 15 keV beam energy, 8.9 mm working distance, and 60 and 120  $\mu\text{m}$  aperture for point analyses or EDS maps respectively.

Along the ~20 km long Mua segment, the BMF scarp is oblique to a gently dipping curvi-planar cohesive foliation in biotite gneisses (Figure 2a). This gneissic foliation is defined by mm-spaced bands of quartz + feldspar alternating with bands of biotite + garnet + hornblende (Figure S2d in the Supporting Information S1). Samples from within 2 m of the 13 m high BMF scarp by the Naminkikowe River, including directly from the scarp itself, contain mm-scale quartzofeldspathic and biotite grains that are locally (15%–30% by area) surrounded by a fine-grained (<10  $\mu\text{m}$  grain size) matrix that consists of fragmented quartzofeldspathic and chlorite grains (Figure 2, Figures S2 and S3 in the Supporting Information S1).

At distances 2–20 m from the scarp, a gently NE-dipping set of joints, with a subordinate subvertical N-S striking joint set, is observed in outcrop (Figure 2c). Here, joint spacing is 0.01–0.1 m but this increases to >0.1 m at distances 20–350 m from the scarp (Figure 2c and Figure S2c in the Supporting Information S1). In all samples 2–350 m from the BMF scarp at Mua, mm-scale quartzofeldspathic grains are crosscut by microfractures, however, there is no evidence for shear displacement across these microfractures. Microfractures are 1–50  $\mu\text{m}$  thick and typically contain a brown fine-grained fill identified using qualitative EDS as chlorite and Fe-oxide (Figures S2 and S4 in the Supporting Information S1). Microfracture density (~1–4 mm<sup>-1</sup>) does not increase with proximity to the fault over our 350 m long transect (Figure 4 and Figure S2 in the Supporting Information S1).

Along the ~20-km long Kasinje segment, the BMF is parallel to a foliation defined by quartzofeldspathic bands alternating with bands of hornblende + garnet + biotite (Figure 3). Adjacent to the 16 m high BMF scarp by the Mtuta River, including in scattered exposure on its immediate hanging wall side, is a 5 m wide interval of fractured rock with 0.1–1 m spaced, foliation-parallel joints (Figure 3b and Figure S5a in the Supporting Information S1). In this macroscopically fractured interval, bands of intact quartzofeldspathic domains and calcite veins are locally interlayered with 10–100  $\mu\text{m}$  bands of fragmented plagioclase and calcite (Figure 3d, Figures S4d and S5b in the Supporting Information S1). No macroscopic, fault-related deformation is observed in the hanging wall more than 16 m from the scarp (Figure 3a and Figure S4f in the Supporting Information S1). Samples from this hanging wall section and >5 m into the footwall contain mm-scale quartzofeldspathic grains that are cross-cut by chlorite veins (Figures S4 and S5 in the Supporting Information S1). Microscale fracture density is 1–4 mm<sup>-1</sup> and does not vary systematically along the 80 m long transect (Figure 4).

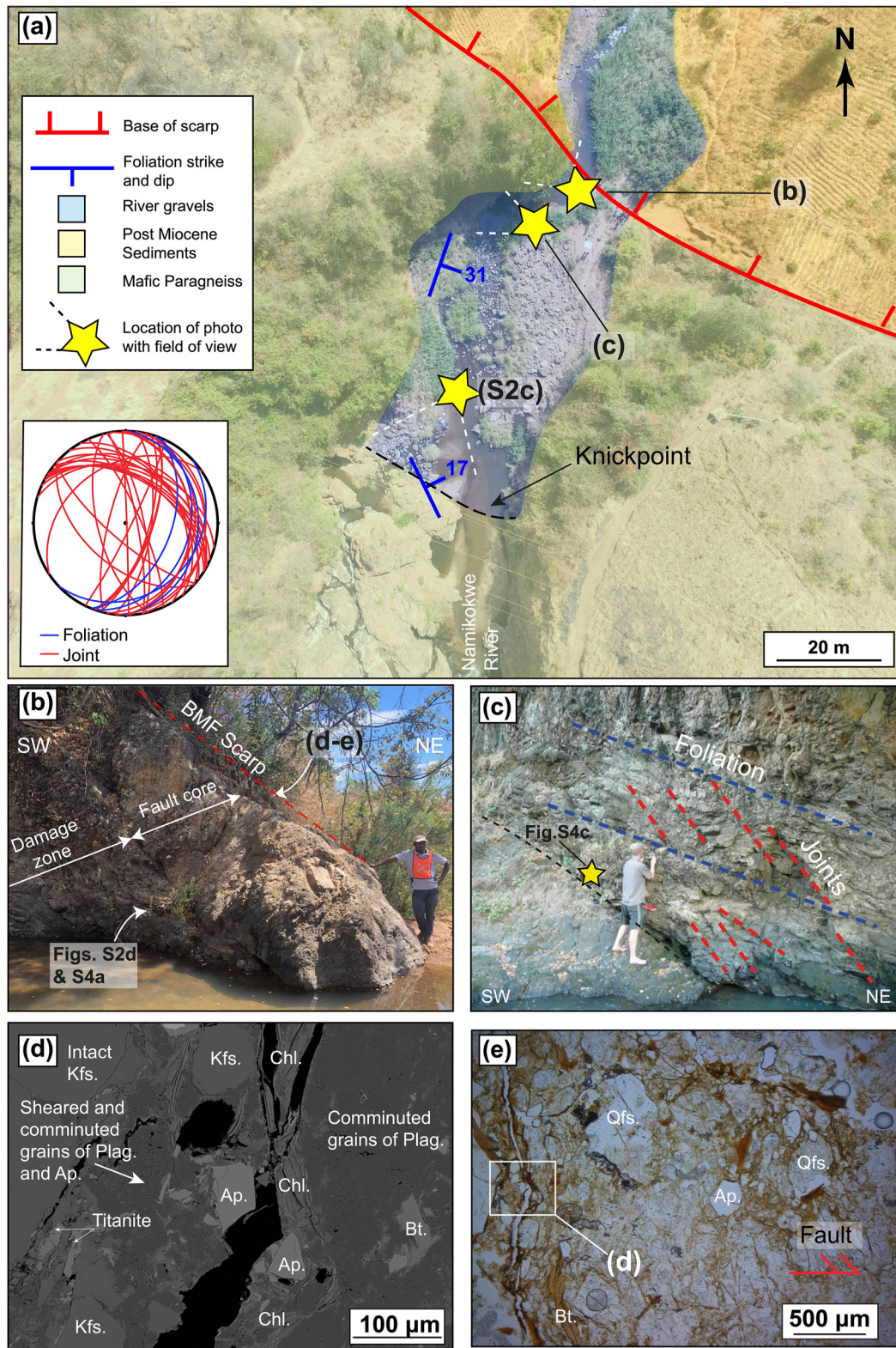


Figure 2.

#### 4. Bilila-Mtakataka Fault Zone Structure

We now place our field and microstructural observations of the BMF in the context of conceptual fault zone structure models (Caine et al., 1996). At Mua, we interpret that the fine-grained matrix observed in a 2 m thick cohesive unit adjacent to the scarp (Figure 2 and Figure S3 in the Supporting Information S1) formed from grain-scale fragmentation and sliding (i.e., comminution) during slip along the BMF. Evidence for displacement along the BMF is localized within this protocataclasite unit (Woodcock & Mort, 2008). This 2 m wide unit provides a minimum fault core width estimate at Mua, because the hanging wall is not exposed at this locality (Figures 2a and 4). We define the BMF footwall damage zone at Mua as the region 2–20 m from the scarp where there is no evidence of grain-scale comminution but relatively closely spaced (0.01–0.1 m) joints are present (Figure 2c). Although the hanging wall damage zone is not exposed at Mua, it is unlikely to be more than three times wider than the 20 m footwall damage zone (Savage & Brodsky, 2011). Therefore, we suggest that the damage zone's total width at Mua is 20–80 m.

A near complete footwall to hanging wall section through the BMF is exposed at Kasinje (Figure 3), however, no distinct gouge or cataclasite layers that would typically define a fault core are observed. We cannot rule out that this is because of incomplete exposure or sampling, although a 2 m thick protocataclasite, as observed at Mua, should have been visible. We interpret that the full width of the BMF damage zone is contained within the localized interval of closely spaced foliation-parallel joints that extends ~5 m from the scarp into the footwall and <16 m into the hanging wall (Figure 3a).

Calcite veins are observed within the damage zone at Kasinje. They are also documented within other nearby fault zones, but not in the background country rock (Wedmore et al., 2020; Williams et al., 2019). We attribute their formation to damage zone fracturing and subsequent mineralization from calcite-saturated meteoric fluids that circulate in the surrounding crust (Dávalos-Elizondo et al., 2021). Veins at Mua and >5 m from the scarp at Kasinje are dominantly made of Fe-oxide and chlorite (Figures S2–S5 in the Supporting Information S1). These minerals are not a common low temperature (<300°C) alteration product (Tulloch, 1979), nor is dissolved iron typical of regional hydrothermal fluids (Dávalos-Elizondo et al., 2021). We therefore suggest these veins, which are the most common microfracture type around the BMF, formed before current rift-related faulting. It is possible that there is another microfracture type that formed due to BMF-related deformation. However, if these microfractures had formed to the extent that is observed in faults in isotropic crust, where their density increases by over an order of magnitude within the damage zone (Anders & Wiltschko, 1994; Mitchell & Faulkner, 2009; Wilson et al., 2003), then we would have expected them to influence the trends in Figure 4.

Fault zone analyses are always limited by erosion of incohesive fault rocks and lack of exposure (Shipton et al., 2019). Nevertheless, at Kasinje the preserved composite scarp shape indicates relatively minor scarp erosion since the most recent earthquake (Hodge et al., 2020). Furthermore, incohesive fault rocks are preserved adjacent to fault scarps in similar environments and rock types elsewhere in southern Malawi (Wedmore et al., 2020; Williams et al., 2019) and in other subtropical regions of the East African Rift's Western Branch (Delvaux et al., 2012; Ring, 1994; Vittori et al., 1997; Wheeler & Karson, 1989).

#### 5. Fault Damage and the Earthquake Energy Budget

We observe a macroscopic damage zone at both Kasinje and Mua. Although there is scatter in data compilations, the ratio between fault displacement and damage zone width is typically ~0.1 for faults with comparable displacement (~10<sup>2</sup>–10<sup>3</sup> m) to the BMF (Savage & Brodsky, 2011; Torabi & Berg, 2011). The 5–20 m wide damage zone at Kasinje, where the BMF is foliation-parallel, is therefore narrow compared to that predicted for a fault with the same displacement in isotropic crust (40–120 m) and to where the BMF is foliation-oblique at Mua (20–80 m).

Variations in fault displacement, pressure-temperature (*P-T*) conditions, and fabric composition can influence fault structure-foliation interactions (see Section 1). However, the BMF has accommodated similar amounts of

---

**Figure 2.** Field site at Mua with microstructural observations of the Bilila-Mtakataka Fault (BMF)-related deformation. (a) Unmanned aerial vehicle photograph overlain by geologic/geomorphic units with (inset) equal area stereonet depicting foliation and joint orientations. (b) Exposure adjacent to the BMF scarp, and (c) damage zone at Mua with <0.1 m spaced joints that are oblique to the foliation. Photo credit: Johann Diener. (d) Backscatter electron image of thin section from sample adjacent to the BMF scarp with comminuted plagioclase (Plag.) and chlorite (Chl.) grains surrounding K-feldspar (Kfs.) clasts. Mineral identification based on EDS map shown in Figure S3a in the Supporting Information S1. Bt.: Biotite, Ap.: Apatite. (e) Photomicrograph in plane polarised light showing context of area shown in (d). Qfs, Quartzofeldspathic porphyroclast.

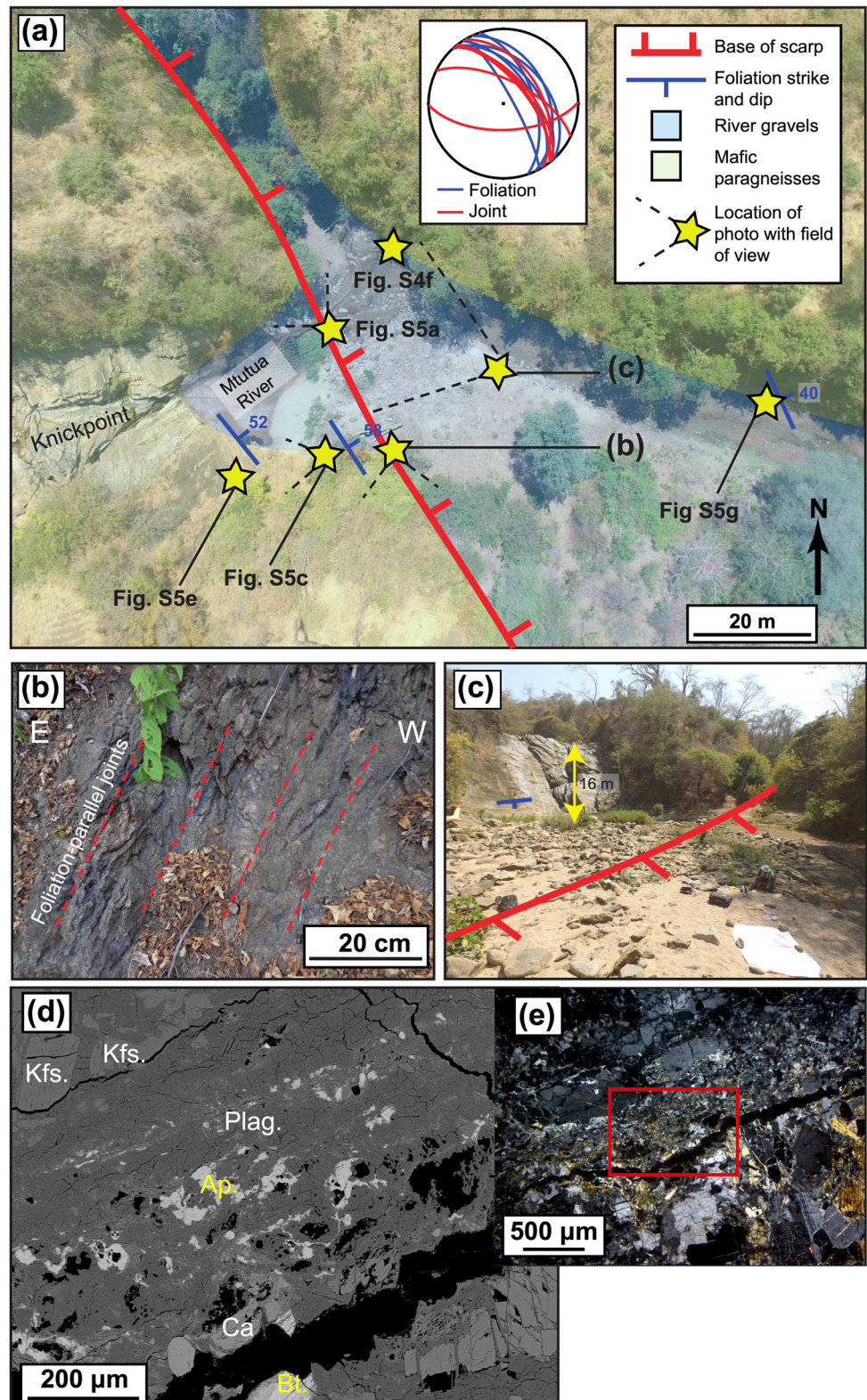


**Figure 3.** Field site at Kasinje with microstructural observations of the Bilila-Mtakataka Fault (BMF)-related deformation: (a) Unmanned aerial vehicle image of site, (b) BMF damage zone exposure (Photo credit: Johann Diener), and (c) oblique view of scarp and knickpoint. (d) Backscattered electron image of fragmented plagioclase (Plag.), calcite (Ca.), and apatite (Ap.) grains from sample adjacent to scarp. Kfs.; K-feldspar, Bt.; Biotite. (e) Photomicrograph of region around (d) taken in Cross Polarised Light.

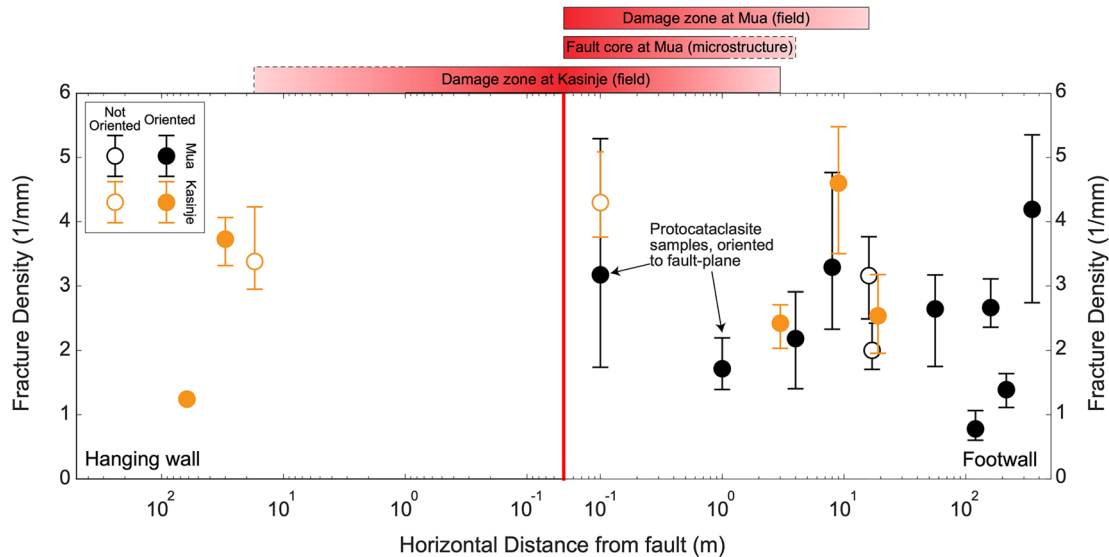


**Figure 4.** Area-weighted average microscale fracture density in quartz and feldspar grains plotted against horizontal distance from the Bilila-Mtakataka Fault scarp. Error bars represent the fracture density range over the three sample areas analyzed within each thin section. Extent of different fault zone structure components also shown for Mua and Kasinje; dashed lines indicate interpretation is based on limited sampling.

displacement at Kasinje and Mua (Hodge et al., 2018; Ojo et al., 2022), both sites reflect deformation at near-surface  $P$ - $T$  conditions, and their metamorphic fabrics and composition are broadly similar. We therefore interpret that the differences in fault zone width between Kasinje and Mua are associated with the BMF's local orientation relative to the surrounding foliation. If true, then earthquakes that reactivate near-surface metamorphic foliations consume less energy by dissipative processes, such as wall rock fracturing, grain scale fragmentation, and frictional sliding (that is,  $E_G$  and  $E_F$  in Equation 1; Shipton et al., 2006), than earthquakes propagating through intact rock or across pre-existing weaknesses. Deep-seated ( $>5$  km depth) pre-existing weaknesses may control the BMF's geometry (Hodge et al., 2018; Williams et al., 2019), and so could also contribute to relatively low earthquake energy dissipation. This could account for the lack of increased microfracturing in both the Kasinje and Mua damage zones compared to low displacement faults in isotropic crust.

Our hypothesis for relatively low earthquake energy dissipation along the BMF implies that the earthquake radiation efficiency ( $\eta_{\text{eff}}$ ), as defined by the ratio of radiated energy ( $E_R$  in Equation 1) to total available earthquake energy (Kanamori & Rivera, 2006), is relatively high. In other fault zones,  $\eta_{\text{eff}}$  has been obtained from seismic waveforms (Kaneko et al., 2017; Venkataraman et al., 2006). However, to directly test our hypothesis by applying this analysis to the BMF ideally require near-fault records of moderate to large earthquakes, which do not currently exist for the BMF (Jackson & Blenkinsop, 1993; Stevens et al., 2021). Nevertheless, ruptures with relatively high  $\eta_{\text{eff}}$  can host more coseismic slip (Kanamori & Rivera, 2006). This is consistent with relatively large single-event displacement:length ratios inferred from topographic profiles across the BMF's scarp (Hodge et al., 2020). Furthermore our hypothesis is supported by comparisons to: (a) relatively low earthquake energy dissipation and a narrow damage zone in places where the 1999  $M_w$  7.6 Chi-Chi earthquake rupture followed sedimentary bedding (Heermance et al., 2003; Wang, 2006), (b) localized damage zones along surface rupturing faults in Australia that are aligned to well-oriented pre-existing weaknesses (Yang et al., 2021), and (c) studies of continental plate boundary faults, which tend to inherit pre-existing weaknesses and exhibit narrow fault cores relative to their displacement (McKay et al., 2021).

Not all faults that follow pre-existing weaknesses exhibit narrow damage zones given their displacement (Table S1 in the Supporting Information S1). We suggest that the limited wall rock fracturing around the BMF reflects the favorable orientation of pre-existing weaknesses to the regional stresses (Figure 1b; Hodge et al., 2018; Williams et al., 2019), and that it has yet to develop thick sequences of mechanically isotropic cataclasites and gouges (Kirkpatrick et al., 2013). The foliation's relatively low phyllosilicate content and cohesive nature around the BMF, which prevents multiple foliation planes from reactivating, may also contribute to this finding (Bistacchi et al., 2010; Fletcher et al., 2020). If these factors combine to increase earthquake  $\eta_{\text{eff}}$  and reduce damage in

other low-displacement foliation-parallel faults, then the ability of these faults to transmit fluids will be reduced (Caine et al., 1996), and they will be more difficult to detect in geophysical surveys (Kelly et al., 2017).

## 6. Conclusions

Using field and microstructural observations, we find that where southern Malawi's Bilila-Mtakataka Fault (BMF) is parallel to surrounding metamorphic foliations, it has a relatively narrow damage zone (5–20 m wide), compared to sites where it is foliation-oblique (20–80 m), and to other faults in isotropic crust with comparable displacement (~40–120 m wide for 0.4–1.2 km displacement fault; Savage & Brodsky, 2011; Torabi & Berg, 2011). Minimal evidence for microfracturing and grain comminution is observed regardless of whether the BMF is parallel or oblique to surface foliations. Our observations from the BMF of poorly developed fault rocks and a narrow damage zone, which are particularly apparent where it is parallel to surface fabrics, can be explained if earthquake slip reactivates favorably oriented pre-existing weaknesses (Hodge et al., 2018; Williams et al., 2019). We propose that compared to a low-displacement fault in intact crust, reactivation of these weaknesses has resulted in less BMF earthquake energy being dissipated into accumulating fault gouge and damage.

## Data Availability Statement

TanDEM-X data were provided through German Aerospace Centre (DLR) proposal DEM\_GEOL0686 and can be obtained from the DLR at: <https://tandemx-science.dlr.de/cgi-bin/wcm.pl?page=TDM-Proposal-Submission-Procedure> (date last accessed 15/02/22). Field data are available via Strabospot <https://strabospot.org/search?c=MzKxNzUxNy42MjY5NTcxODU2eC0xNzgzMDY1LjE1MzE5MzKxMjd4Ny45OTMzMzMzMzMzMzMzMzI=> (data last accessed 02/19/2020).

## Acknowledgments

This work is supported by the EPSRC-Global Challenges Research Fund PREPARE (EP/P028233/1) and SAFER-PREPARED (EP/T015462/1) projects. Figures 2c and 3b were provided by Johann Diener. The authors gratefully acknowledge Zoe Shipton and Jessica McBeck for providing constructive and thoughtful reviews, and Bob Holdsworth for comments on an earlier manuscript version. The authors also thank Antony Oldroyd and Duncan Muir for preparing thin sections and assistance with the Scanning Electron Microscope respectively. Open access publishing facilitated by University of Otago, as part of the Wiley - University of Otago agreement via the Council of Australian University Librarians.

## References

- Accardo, N. J., Shillington, D. J., Gaherty, J. B., Scholz, C. A., Nyblade, A. A., & Chindandali, P. R. N. (2018). Constraints on rift basin structure and border fault growth in the northern Malawi rift from 3-D seismic refraction imaging. *Journal of Geophysical Research: Solid Earth*, 123(11), 10003–10025. <https://doi.org/10.1029/2018JB016504>
- Allen, J. L. (2005). A multi-kilometer pseudotachylite system as an exhumed record of earthquake rupture geometry at hypocentral depths (Colorado, USA). *Tectonophysics*, 402(1–4), 37–54. <https://doi.org/10.1016/j.tecto.2004.10.017>
- Anders, M. H., & Wiltschko, D. V. (1994). Microfracturing, paleostress and the growth of faults. *Journal of Structural Geology*, 16(6), 795–815. [https://doi.org/10.1016/0191-8141\(94\)90146-5](https://doi.org/10.1016/0191-8141(94)90146-5)
- Beacom, L. E., Holdsworth, R. E., McCaffrey, K. J. W., & Anderson, T. B. (2001). *A quantitative study of the influence of pre-existing compositional and fabric heterogeneities upon fracture-zone development during basement reactivation* (Vol. 186, pp. 195–211). Geological Society Special Publication. <https://doi.org/10.1144/GSL.SP.2001.186.01.12>
- Bistacchi, A., Massironi, M., & Menegon, L. (2010). Three-dimensional characterization of a crustal-scale fault zone: The Pusteria and Sprechenstein fault system (Eastern Alps). *Journal of Structural Geology*, 32(12), 2022–2041. <https://doi.org/10.1016/j.jsg.2010.06.003>
- Butler, R. W. H., Bond, C. E., Shipton, Z. K., Jones, R. R., & Casey, M. (2008). Fabric anisotropy controls faulting in the continental crust. *Journal of the Geological Society*, 165(2), 449–452. <https://doi.org/10.1144/0016-76492007-129>
- Caine, J. S., Evans, J. P., & Forster, C. B. (1996). Fault zone architecture and permeability structure. *Geology*, 24(11), 1025–1028. [https://doi.org/10.1130/0091-7613\(1996\)024<1025:fzaaps>2.3.co;2](https://doi.org/10.1130/0091-7613(1996)024<1025:fzaaps>2.3.co;2)
- Callahan, O. A., Eichhubl, P., & Davatzes, N. C. (2020). Mineral precipitation as a mechanism of fault core growth. *Journal of Structural Geology*, 140. <https://doi.org/10.1016/j.jsg.2020.104156>
- Cartwright, J. A., Trudgill, B. D., & Mansfield, C. S. (1995). Fault growth by segment linkage: An explanation for scatter in maximum displacement and trace length data from the Canyonlands Grabens of SE Utah. *Journal of Structural Geology*, 17(9), 1319–1326. [https://doi.org/10.1016/0191-8141\(95\)00033-A](https://doi.org/10.1016/0191-8141(95)00033-A)
- Chester, J. S., Chester, F. M., & Kronenberg, A. K. (2005). Fracture surface energy of the Punchbowl fault, San Andreas system. *Nature*, 437(7055), 133–136. <https://doi.org/10.1038/nature03942>
- Childs, C., Manzocchi, T., Walsh, J. J., Bonson, C. G., Nicol, A., & Schöpfer, M. P. J. (2009). A geometric model of fault zone and fault rock thickness variations. *Journal of Structural Geology*, 31(2), 117–127. <https://doi.org/10.1016/j.jsg.2008.08.009>
- Collanega, L., Siuda, K., Jackson, A.-L. C., Bell, R. E., Coleman, A. J., Lenhart, A., et al. (2019). Normal fault growth influenced by basement fabrics: The importance of preferential nucleation from pre-existing structures. *Basin Research*, 31(4), 659–687. <https://doi.org/10.1111/bre.12327>
- Crider, J. G., & Peacock, D. C. P. (2004). Initiation of brittle faults in the upper crust: A review of field observations. *Journal of Structural Geology*, 26(4), 691–707. <https://doi.org/10.1016/j.jsg.2003.07.007>
- Dávalos-Elizondo, E., Atekwana, E. A., Atekwana, E. A., Tsokonombwe, G., & Laó-Dávila, D. A. (2021). Medium to low enthalpy geothermal reservoirs estimated from geothermometry and mixing models of hot springs along the Malawi Rift Zone. *Geothermics*, 89. <https://doi.org/10.1016/j.geothermics.2020.101963>
- Dawson, A. L., & Kirkpatrick, I. M. (1968). *The geology of the Cape Maclear peninsula and lower Bwanje valley* (Vol. 28). Malawi: Bulletin of the Geological Survey.

- Delvaux, D., Kervyn, F., Macheyeki, A. S., & Temu, E. B. (2012). Geodynamic significance of the TRM segment in the East African Rift (W-Tanzania): Active tectonics and paleostress in the Ufipa plateau and rukwa basin. *Journal of Structural Geology*, 37, 161–180. <https://doi.org/10.1016/j.jsg.2012.01.008>
- Donath, F. A. (1961). Experimental study of shear failure in anisotropic rocks. *Geological Society of America Bulletin*, 72, 985–989. <https://doi.org/10.1130/0016-7606%281961%2972%5B985:esosfi%5D2.0.co;2>
- Fang, Z., & Dunham, E. M. (2013). Additional shear resistance from fault roughness and stress levels on geometrically complex faults. *Journal of Geophysical Research: Solid Earth*, 118(7), 3642–3654. <https://doi.org/10.1002/jgrb.50262>
- Faulkner, D. R., Mitchell, T. M., Rutter, E. H., & Cembrano, J. (2008). On the structure and mechanical properties of large strike-slip faults. *Geological Society Special Publication*, 299(1), 139–150. <https://doi.org/10.1144/SP299.9>
- Fletcher, J. M., Teran, O. J., Rockwell, T. K., Oskin, M. E., Hudnut, K. W., Spelz, R. M., et al. (2020). An analysis of the factors that control fault zone architecture and the importance of fault orientation relative to regional stress. *GSA Bulletin*, 1–21. <https://doi.org/10.1130/b35308.1>
- Healy, D., Rizzo, R. E., Cornwell, D. G., Farrell, N. J. C., Watkins, H., Timms, N. E., et al. (2017). FracPaQ: A MATLAB™ toolbox for the quantification of fracture patterns. *Journal of Structural Geology*, 95, 1–16. <https://doi.org/10.1016/j.jsg.2016.12.003>
- Hecker, S., DeLong, S. B., & Schwartz, D. P. (2021). Rapid strain release on the bear river fault zone, Utah–Wyoming—the impact of preexisting structure on the rupture behavior of a new normal fault. *Tectonophysics*, 808, 228819. <https://doi.org/10.1016/j.tecto.2021.228819>
- Heermance, R., Shipton, Z. K., & Evans, J. P. (2003). Fault structure control on fault slip and ground motion during the 1999 rupture of the Chelungpu fault, Taiwan. *Bulletin of the Seismological Society of America*, 93(3), 1034–1050. <https://doi.org/10.1785/0120010230>
- Hodge, M., Biggs, J., FagerengMdala, H., Wedmore, L. N. J., & Williams, J. N. (2020). Evidence from high-resolution topography for multiple earthquakes on high slip-to-length fault scarps: The Bilila-Mtakataka Fault, Malawi. *Tectonics*, 39(2), e2019TC005933. <https://doi.org/10.1029/2019TC005933>
- Hodge, M., Fagereng, A., Biggs, J., & Mdala, H. (2018). Controls on early-rift geometry: New perspectives from the Bilila-Mtakataka Fault, Malawi. *Geophysical Research Letters*, 45(9), 3896–3905. <https://doi.org/10.1029/2018GL077343>
- Jackson, J., & Blenkinsop, T. (1993). The Malaŵi earthquake of March 10, 1989: Deep faulting within the East African rift system. *Tectonics*, 12(5), 1131–1139. <https://doi.org/10.1029/93TC01064>
- Jackson, J., & Blenkinsop, T. (1997). The Bilila-Mtakataka Fault in Malawi: An active, 100-km long, normal fault segment in thick seismogenic crust. *Tectonics*, 16(1), 137–150. <https://doi.org/10.1029/96TC02494>
- Kanamori, H., & Rivera, L. (2006). Energy partitioning during an earthquake. *Earthquakes: Radiated Energy and the Physics of Faulting*, 170, 3–13. <https://doi.org/10.1029/170GM03>
- Kaneko, Y., Fukuyama, E., & Hamling, I. J. (2017). Slip-weakening distance and energy budget inferred from near-fault ground deformation during the 2016  $M_w$  7.8 Kaikōura earthquake. *Geophysical Research Letters*, 44(10), 4765–4773. <https://doi.org/10.1002/2017GL073681>
- Kelly, C. M., Faulkner, D. R., & Rietbrock, A. (2017). Seismically invisible fault zones: Laboratory insights into imaging faults in anisotropic rocks. *Geophysical Research Letters*, 44(16), 8205–8212. <https://doi.org/10.1002/2017GL073726>
- Kirkpatrick, J. D., Bezerra, F. H. R., Shipton, Z. K., Do Nascimento, A. F., Pytharouli, S. I., Lunn, R. J., & Soden, A. M. (2013). Scale-dependent influence of pre-existing basement shear zones on rift faulting: A case study from NE Brazil. *Journal of the Geological Society*, 170(2), 237–247. <https://doi.org/10.1144/jgs2012-043>
- Lacroix, B., Tessei, T., Oliot, E., Lahfid, A., & Colletini, C. (2015). Early weakening processes inside thrust fault. *Tectonics*. <https://doi.org/10.1002/2014TC003716>
- Lockner, D. A., Byerlee, J. D., Kuksenko, V., Ponomarev, A., & Sidorin, A. (1991). Quasi-static fault growth and shear fracture energy in granite. *Nature*, 350(6313), 39–42. <https://doi.org/10.1038/350039a0>
- Ma, K.-F., Tanaka, H., Song, S.-R., Wang, C.-Y., Hung, J.-H., Tsai, Y.-B., et al. (2006). Slip zone and energetics of a large earthquake from the Taiwan Chelungpu-fault drilling project. *Nature*, 444(7118), 473–476. <https://doi.org/10.1038/nature05253>
- McBeck, J. A., Ben-Zion, Y., & Renard, F. (2021). How the force and fracture architectures develop within and around healed fault zones during biaxial loading toward macroscopic failure. *Journal of Structural Geology*, 147, 104329. <https://doi.org/10.1016/j.jsg.2021.104329>
- McBeck, J. A., Mair, K., & Renard, F. (2019). Linking macroscopic failure with micromechanical processes in layered rocks: How layer orientation and roughness control macroscopic behavior. *Tectonophysics*, 750, 229–242. <https://doi.org/10.1016/j.tecto.2018.11.016>
- McKay, L., Lunn, R. J., Shipton, Z. K., Pytharouli, S., & Roberts, J. J. (2021). Do intraplate and plate boundary fault systems evolve in a similar way with repeated slip events? *Earth and Planetary Science Letters*, 559, 116757. <https://doi.org/10.1016/j.epsl.2021.116757>
- Micklethwaite, S., & Cox, S. F. (2004). Fault-segment rupture, aftershock-zone fluid flow, and mineralization. *Geology*, 32(9), 813–816. <https://doi.org/10.1130/g20559.1>
- Misra, S., Ellis, S., & Mandal, N. (2015). Fault damage zones in mechanically layered rocks: The effects of planar anisotropy. *Journal of Geophysical Research: Solid Earth*, 120(8), 5432–5452. <https://doi.org/10.1002/2014JB011780>
- Mitchell, T. M., & Faulkner, D. R. (2009). The nature and origin of off-fault damage surrounding strike-slip fault zones with a wide range of displacements: A field study from the Atacama fault system, northern Chile. *Journal of Structural Geology*, 31(8), 802–816. <https://doi.org/10.1016/j.jsg.2009.05.002>
- Niemeijer, A., Di Toro, G., Griffith, A. W., Bistacchi, A., Smith, S. A. F., & Nielsen, S. (2012). Inferring earthquake physics and chemistry using an integrated field and laboratory approach. *Journal of Structural Geology*, 39, 2–36. <https://doi.org/10.1016/j.jsg.2012.02.018>
- Ojo, O. O., Ohenhen, L. O., Kolawole, F., Johnson, S. G., Chindandali, P. R., Atekwana, E. A., & Laó-Dávila, D. A. (2022). Under-Displaced Normal Faults: Strain Accommodation Along an Early-Stage Rift-Bounding Fault in the Southern Malawi Rift. *Frontiers in Earth Science*, 10, 846389. <https://doi.org/10.3389/feart.2022.846389>
- Paton, D. A. (2006). Influence of crustal heterogeneity on normal fault dimensions and evolution: Southern South Africa extensional system. *Journal of Structural Geology*, 28(5), 868–886. <https://doi.org/10.1016/j.jsg.2006.01.006>
- Perrin, C., Manighetti, I., Ampuero, J. P., Cappa, F., & Gaudemer, Y. (2016). Location of largest earthquake slip and fast rupture controlled by along-strike change in fault structural maturity due to fault growth. *Journal of Geophysical Research: Solid Earth*, 121(5), 3666–3685. <https://doi.org/10.1002/2015JB012671>
- Renard, F., Weiss, J., Mathiesen, J., Ben-Zion, Y., Kandula, N., & Cordonnier, B. (2018). Critical evolution of damage toward system-size failure in crystalline rock. *Journal of Geophysical Research: Solid Earth*, 123(2), 1969–1986. <https://doi.org/10.1002/2017JB014964>
- Ring, U. (1994). The influence of preexisting structure on the evolution of the Cenozoic Malawi rift (East African rift system). *Tectonics*, 13(2), 313–326. <https://doi.org/10.1029/93TC03188>
- Rotevatn, A., Jackson, C. A. L., Tvedt, A. B. M., Bell, R. E., & Blækkan, I. (2019). How do normal faults grow? *Journal of Structural Geology*, 125, 174–184. <https://doi.org/10.1016/j.jsg.2018.08.005>
- Sagy, A., Brodsky, E. E., & Axen, G. J. (2007). Evolution of fault surface roughness with slip. *Geology*, 35(3), 283–286. <https://doi.org/10.1130/G23235A.1>

- Savage, H. M., & Brodsky, E. E. (2011). Collateral damage: Evolution with displacement of fracture distribution and secondary fault strands in fault damage zones. *Journal of Geophysical Research*, *116*(3), B03405. <https://doi.org/10.1029/2010JB007665>
- Savage, H. M., & Cooke, M. L. (2010). Unlocking the effects of friction on fault damage zones. *Journal of Structural Geology*, *32*(11), 1732–1741. <https://doi.org/10.1016/j.jsg.2009.08.014>
- Scholz, C. A., Shillington, D. J., Wright, L. J. M., Accardo, N., Gaherty, J. B., & Chindandali, P. (2020). Intrarift fault fabric, segmentation, and basin evolution of the Lake Malawi (Nyasa) Rift, East Africa. *Geosphere*, *16*(5), 1293–1311. <https://doi.org/10.1130/GES02228.1>
- Schwanghart, W., & Scherler, D. (2014). Short communication: Topotoolbox 2 – MATLAB-based software for topographic analysis and modeling in earth surface sciences. *Earth Surface Dynamics*, *2*(1), 1–7. <https://doi.org/10.5194/esurf-2-1-2014>
- Shipton, Z. K., Evans, J. P., Abercrombie, R. E., & Brodsky, E. E. (2006). The missing sinks: Slip localization in faults, damage zones, and the seismic energy budget. *Geophysical Monograph Series*, *170*, 217–222. <https://doi.org/10.1029/170GM22>
- Shipton, Z. K., Roberts, J., Comrie, E., Kremer, Y., Lunn, R., & Caine, J. (2019). *Fault fictions: Cognitive biases in the conceptualization of fault zones*. Geological Society Special Publications.
- Sibson, R. H. (1977). Fault rocks and fault mechanisms. *Journal of the Geological Society*, *133*(3), 191–213. <https://doi.org/10.1144/gsjgs.133.3.0191>
- Soden, A. M., Shipton, Z. K., Lunn, R. J., Pytharoulis, S. I., Kirkpatrick, J. D., Do Nascimento, A. F., & Bezerra, F. H. R. (2014). Brittle structures focused on subtle crustal heterogeneities: Implications for flow in fractured rocks. *Journal of the Geological Society*, *171*(4), 509–524. <https://doi.org/10.1144/jgs2013-051>
- Stevens, V. L., Sloan, R. A., Chindandali, P. R., Wedmore, L. N. J., Salomon, G. W., & Muir, R. A. (2021). The entire crust can be seismogenic: Evidence from southern Malawi. *Tectonics*, *40*(6), e2020TC006654. <https://doi.org/10.1029/2020tc006654>
- Tien, Y. M., Kuo, M. C., & Juang, C. H. (2006). An experimental investigation of the failure mechanism of simulated transversely isotropic rocks. *International Journal of Rock Mechanics and Mining Sciences*, *43*(8), 1163–1181. <https://doi.org/10.1016/j.ijrmm.2006.03.011>
- Tinti, E., Spudich, P., & Cocco, M. (2005). Earthquake fracture energy inferred from kinematic rupture models on extended faults. *Journal of Geophysical Research*, *110*(12), 1–25. <https://doi.org/10.1029/2005JB003644>
- Torabi, A., & Berg, S. S. (2011). Scaling of fault attributes: A review. *Marine and Petroleum Geology*. <https://doi.org/10.1016/j.marpetgeo.2011.04.003>
- Torabi, A., Ellingsen, T. S. S., Johannessen, M. U., Alaei, B., Rotevatn, A., & Chiarella, D. (2020). Fault zone architecture and its scaling laws: Where does the damage zone start and stop? *Geological Society, London, Special Publications*, *496*(1), 99–124. <https://doi.org/10.1144/sp496-2018-151>
- Tulloch, A. J. (1979). Secondary Ca-Al silicates as low-grade alteration products of granitoid biotite. *Contributions to Mineralogy and Petrology*, *69*(2), 105–117. <https://doi.org/10.1007/BF00371854>
- Venkataraman, A., Beroza, G. C., & Boatwright, J. (2006). A brief review of techniques used to estimate radiated seismic energy. *Earthquakes: Radiated Energy and the Physics of Faulting*, *170*, 15–24. <https://doi.org/10.1029/170GM04>
- Vittori, E., Delvaux, D., & Kervyn, F. (1997). Kanda fault: A major seismogenic element west of the rukwa rift (Tanzania, East Africa). *Journal of Geodynamics*, *24*(1–4), 139–153. [https://doi.org/10.1016/S0264-3707\(96\)00038-5](https://doi.org/10.1016/S0264-3707(96)00038-5)
- Walsh, J. J., Nicol, A., & Childs, C. (2002). An alternative model for the growth of faults. *Journal of Structural Geology*, *24*(11), 1669–1675. [https://doi.org/10.1016/S0191-8141\(01\)00165-1](https://doi.org/10.1016/S0191-8141(01)00165-1)
- Walshaw, R. D. (1965). The geology of the Nchue-balaka area. *Bulletin of the Geological Survey, Malawi*, *19*.
- Wang, J. H. (2006). A review of the source parameters of the 1999 Ms 7.6 chi-chi, Taiwan, earthquake. *Terrestrial, Atmospheric and Oceanic Sciences*, *17*(1), 179–202. [https://doi.org/10.3319/tao.2006.17.1.179\(t\)](https://doi.org/10.3319/tao.2006.17.1.179(t))
- Wedmore, L. N. J., Biggs, J., Floyd, M., FagerengMdala, H., Chindandali, P., Williams, J. N., et al. (2021). Geodetic constraints on cratonic microplates and broad strain during rifting of thick southern African lithosphere. *Geophysical Research Letters*, *48*(17). <https://doi.org/10.1029/2021GL093785>
- Wedmore, L. N. J., Williams, J. N., Biggs, J., Fagereng, Å., Mphepo, F., Dulanya, Z., et al. (2020). Structural inheritance and border fault reactivation during active early-stage rifting along the Thyolo fault, Malawi. *Journal of Structural Geology*, *139*, 104097. <https://doi.org/10.1016/j.jsg.2020.104097>
- Wheeler, W. H., & Karson, J. A. (1989). Structure and kinematics of the livingstone mountains border fault zone, Nyasa (Malawi) Rift, southwestern Tanzania. *Journal of African Earth Sciences*, *8*(2–4), 393–413. [https://doi.org/10.1016/S0899-5362\(89\)80034-X](https://doi.org/10.1016/S0899-5362(89)80034-X)
- Williams, J. N., Fagereng, Å., Wedmore, L. N. J., Biggs, J., Mphepo, F., Dulanya, Z., et al. (2019). How do variably striking faults reactivate during rifting? Insights from southern Malawi. *Geochemistry, Geophysics, Geosystems*, *20*(7), 3588–3607. <https://doi.org/10.1029/2019GC008219>
- Williams, J. N., Toy, V. G., Massiot, C., McNamara, D. D., Smith, S. A. F., & Mills, S. (2018). Controls on fault zone structure and brittle fracturing in the foliated hanging wall of the Alpine Fault. *Solid Earth*, *9*(2), 469–489. <https://doi.org/10.5194/se-9-469-2018>
- Wilson, B., Dewers, T., Reches, Z., & Brune, J. (2005). Particle size and energetics of gouge from earthquake rupture zones. *Nature*, *434*(7034), 749–752. <https://doi.org/10.1038/nature03433>
- Wilson, J. E., Chester, J. S., & Chester, F. M. (2003). Microfracture analysis of fault growth and wear processes, Punchbowl Fault, San Andreas system, California. *Journal of Structural Geology*, *25*(11), 1855–1873. [https://doi.org/10.1016/S0191-8141\(03\)00036-1](https://doi.org/10.1016/S0191-8141(03)00036-1)
- Woodcock, N. H., & Mort, K. (2008). Classification of fault breccias and related fault rocks. *Geological Magazine*, *145*(03), 435–440. <https://doi.org/10.1017/S0016756808004883>
- Yang, H., Quigley, M., & King, T. (2021). Surface slip distributions and geometric complexity of intraplate reverse-faulting earthquakes. *Bulletin of the Geological Society of America*, *133*(9–10), 1909–1929. <https://doi.org/10.1130/B35809.1>
- Zangerl, C., Loew, S., & Eberhardt, E. (2006). Structure, geometry and formation of brittle discontinuities in anisotropic crystalline rocks of the central Gotthard massif, Switzerland. *Eclogae Geologicae Helvetiae*, *99*(2), 271–290. <https://doi.org/10.1007/s00015-006-1190-0>